1999

Chemical characteristics of air from differing source regions during the Pacific Exploratory Mission-Tropics A (PEM-Tropics A)

Ashley S. Board

Henry E. Fuelberg

Gerald L. Gregory

Brian G. Heikes
University of Rhode Island, bheikes@uri.edu

Martin G. Schultz

See next page for additional authors

Citation/Publisher Attribution

Board, A. S., H. E. Fuelberg, G. L. Gregory, B. G. Heikes, M. G. Schultz, D. R. Blake, J. E. Dibb, S. T. Sandholm, and R. W. Talbot (1999), Chemical characteristics of air from differing source regions during the Pacific Exploratory Mission-Tropics A (PEM-Tropics A), *J. Geophys. Res.*, 104(D13), 16181–16196, doi: 10.1029/1999JD900021.
Available at: https://doi.org/10.1029/1999JD900021

Chemical characteristics of air from differing source regions during the Pacific Exploratory Mission-Tropics A (PEM-Tropics A)

Authors

Ashley S. Board, Henry E. Fuelberg, Gerald L. Gregory, Brian G. Heikes, Martin G. Schultz, Donald R. Blake, Jack E. Dibb, Scott T. Sandholm, and Robert W. Talbot

JOURNAL OF GEOPHYSICAL RESEARCH, VOL. 104, NO. D13, PAGES 16,181–16,196, JULY 20, 1999

Chemical characteristics of air from differing source regions during the Pacific Exploratory Mission-Tropics A (PEM-Tropics A)

Ashley S. Board,[1] Henry E. Fuelberg,[1] Gerald L. Gregory,[2] Brian G. Heikes,[3]
Martin G. Schultz,[4] Donald R. Blake,[5] Jack E. Dibb,[6]
Scott T. Sandholm,[7] and Robert W. Talbot[6]

Abstract. Ten-day backward trajectories are used to determine the origins of air parcels arriving at airborne DC-8 chemical measurement sites during NASA's Pacific Exploratory Mission-Tropics A (PEM-T) that was conducted during August–October 1996. Those sites at which the air had a common geographical origin and transport history are grouped together, and statistical measures of chemical characteristics are computed. Temporal changes in potential temperature are used to determine whether trajectories experience a significant convective influence during the 10-day period. Those trajectories that do not experience a significant convective influence are divided into four geographical categories depending on their origins and paths. Air parcels originating over Africa and South America are characterized by enhanced mixing ratios of O_3, CO, HNO_3, and PAN. The backward trajectories travel at high altitudes (~10–11 km), covering long distances due to strong upper-tropospheric westerly winds. The observed enhancement of combustion-related species is attributed to biomass burning from distant sources to the west, extending even to South America. The relatively large value of Be-7 probably is due either to less efficient removal of aerosols from upper tropospheric air or to small stratospheric contributions. Aged marine parcels are found to have relatively small concentrations of burning-related species. Although these trajectories arrive at a wide range of aircraft altitudes, they do not pass over a land mass during the preceding 10-day period. Air passing over Australia but no other land mass exhibits a combustion signature; however, photochemical product species such as O_3 and PAN are less enhanced than in the long-range transport category. These trajectories travel shorter distances and are at lower altitudes (~5–8 km) than those reaching Africa and/or South America. The combustion influence on these parcels is attributed to biomass burning emissions injected over Australia. That burning is less widespread than in Africa and South America. Finally, trajectories originating over Southeast Asia appear to receive a weak combustion influence. However, compared to Africa and South America, Southeast Asia has a relatively small incidence of biomass burning. There is little combustion input from Australia due to the high transport altitudes compared to the lower heights of the convection. The Southeast Asian parcels exhibit the greatest NO_x to ΣNO_t ratio of any category, perhaps due to lightning. Parcels experiencing a significant convective influence also are examined. Most of these parcels pass through widespread, persistent convection along either the South Pacific Convergence Zone or Intertropical Convergence Zone approximately 5 days prior to arriving at the aircraft locations. Thus the category mostly represents marine convection. Mixing ratios of peroxides and acids in the convective category are found to be smaller than in parcels not experiencing convection. Small mixing ratios of Be-7 and Pb-210 suggest particle removal by precipitation.

[1]Department of Meteorology, Florida State University, Tallahassee.
[2]NASA Langley Research Center, Hampton, Virginia.
[3]Graduate School of Oceanography, University of Rhode Island, Narragansett.
[4]Department of Earth and Planetary Sciences, Harvard University, Cambridge, Massachusetts.
[5]Department of Chemistry, University of California, Irvine.
[6]Institute for the Study of Earth, Oceans, and Space, University of New Hampshire, Durham.
[7]Department of Earth and Atmospheric Sciences, Georgia Institute of Technology, Atlanta.

Paper number 1999JD900021.
0148-0227/99/1999JD900021$09.00

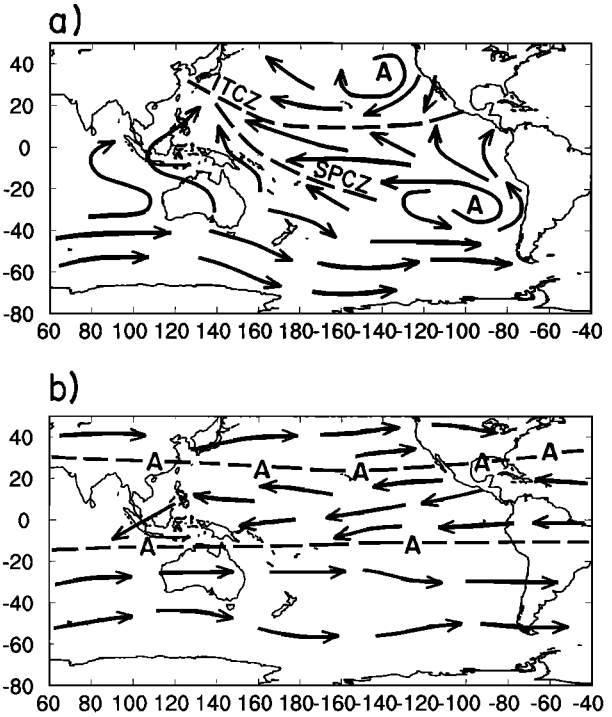

Figure 1. Schematic showing mean streamlines during PEM-T (August 14 to October 6, 1996) for (a) 1000 and (b) 500 hPa. Locations of the ITCZ and SPCZ are indicated by dashed lines at 1000 hPa, while the subtropical anticyclones are denoted "A." At 500 hPa, anticyclonic circulation centers are indicated as A, while ridge lines are dashed.

1. Introduction

Relationships between the origins of tropospheric air parcels, their transport histories, and their chemical characteristics often are not well known. This is especially true for remote regions of the world where both meteorological and chemical data are limited and where the transport time from source regions is many days. The southern Pacific Ocean Basin, the focus of NASA's Pacific Exploratory Mission-Tropics A (PEM-T), is such a region. *Hoell et al.* [1999] provide a complete description of PEM-T. It was conducted from August 14 to October 6, 1996, during the southern hemispheric dry season, using two NASA aircraft, the DC-8 and P-3B.

Fuelberg et al. [1999] give a detailed discussion of meteorological conditions that were important to long-range transport during the PEM-T period. Therefore only major features are repeated here. At 1000 hPa (Figure 1a), subtropical anticyclones dominated both the North and South Pacific Oceans (denoted "A"). These anticyclonic regions generally were devoid of clouds, containing temperature inversions in the lower troposphere because of their subsiding motion. The resulting southeasterly and northeasterly trade winds in the tropical southern and northern hemispheres, respectively, produced an area of low-level convergence near 10°N, that is, the Intertropical Convergence Zone (ITCZ). Ascending motion along the ITCZ produced widespread clouds and convective precipitation. Similarly, the South Pacific Convergence Zone (SPCZ) [*Vincent*, 1994] was a region of ascending motion and extensive cloudiness and precipitation. The SPCZ extended southeastward from the western portion of the ITCZ to near Tahiti (18°S, 150°W). The ITCZ and westernmost portion of the SPCZ merged into one convergence line near the Philippines.

Mean middle tropospheric flow patterns (500 hPa, ~5.5 km mean sea level (msl), Figure 1b) included several subtropical anticyclones near 30°N and 15°S. Ridge axes extending west-east from these centers encompassed nearly the entire North and South Pacific Basins. The ridge lines and anticyclones produced westerly winds north of ~30°N and south of ~15°S, that is, the prevailing westerlies. However, the tropical latitudes in between were dominated by easterly winds. Flow patterns were similar at 300 hPa (~9 km, not shown). The southern subtropical jet stream was located near 30°S, exhibiting only small day-to-day changes in intensity and location. Maximum mean wind speeds >40 m s^{-1} were located over southwestern Australia. The polar jet stream exhibited large day-to-day variability in both speed and location.

Meteorological conditions greatly influence the transport of by-products from regions of biomass burning. Major areas of biomass burning over southern Africa, South America, Australia, and Indonesia during austral spring have been documented by *Hao and Liu* [1994], *Hurst et al.* [1996], *Elvidge and Baugh* [1996], *Fishman et al.* [1996], and *Olson et al.* [1999]. The burning over southern Africa and South America generally is much greater than over Australia and Indonesia (European Space Agency, Global Fire Atlas, 1998, available at http://shark1.esrin.esa.it/FIRE/fire.html). Air frequently recirculates over the burning regions of southern Africa before leaving the eastern African coast and traveling into the Indian Ocean [*Garstang et al.*, 1996; *Tyson et al.*, 1996]. *Thompson et al.* [1996] also concluded that air frequently is transported eastward from Africa into the Indian Ocean. This air can reach the South Pacific Basin, the region of PEM-T [*Fuelberg et al.*, 1999; *Schultz et al.*, 1999; *Vay et al.*, 1999], thereby increasing trace gas concentrations in the region. *Schultz et al.* [1999] noted that a significant increase in tropospheric O_3 over the tropical South Pacific Ocean resulted from biomass burning over Brazil and southern Africa.

By-products of biomass burning can be transported aloft by deep convection [*Pickering et al.*, 1990, 1991, 1992, 1996]. Detailed discussions of this process also are provided by *Chatfield and Delany* [1990] and *Scala et al.* [1990]. Once carried aloft by convection, the burning by-products can be transported quickly to distant locations by the relatively strong upper-tropospheric winds.

Concentrations and lifetimes of most chemical species in the atmosphere are affected by (1) the location where source emissions are injected (i.e., transport time to the region of study), (2) the mechanism of injection (i.e., injected as fresh emissions at high, dry transport altitudes or injected at low altitudes and then transported aloft), and (3) the surrounding environment (particularly temperature, moisture, and solar conditions) during transport. For example, in the marine boundary layer (MBL), the lifetime of O_3 is only 2–5 days [*Fishman et al.*, 1991], whereas it increases to ~90 days in the middle troposphere where the air is drier. Thus dry air aloft, often associated with large-scale subsidence, helps maintain continental pollution plumes for long periods of time. Consequently, long-range transport of these plumes is possible if the pollutants rise out of the boundary layer and into the middle or upper troposphere where there is relatively dry air and strong wind speeds [*Krishnamurti et al.*, 1993].

The objective of this paper is to investigate relations between the origins of air parcels, their transport histories, and

their chemical characteristics during the PEM-T period. We examine 14 DC-8 flights that traversed the southern hemisphere north of 35°S (Figure 2). *Hoell et al.* [1999] describe these flights in detail. Each flight ranged from 8–10 hours duration at altitudes from 0.2–12 km. They traversed an area from near Easter Island west to the Solomon Islands, and from Hawaii south to New Zealand. We use 10-day backward trajectories to determine the origins of air parcels. Parcels having common origins and transport histories are grouped together, and their chemical characteristics measured by the DC-8 are evaluated. This procedure is the reverse of using trajectories to determine the origins of air parcels having a particular chemical signature. Although all chemical species measured aboard the DC-8 were considered, we will focus on species that are most important to the given geographical categories. Previous studies that have used somewhat similar approaches include *Gregory et al.* [1996, 1999] and *Talbot et al.* [1994, 1996a, b, 1997].

2. Data and Methodology

2.1. Meteorological Data

The global gridded meteorological data used for this research were prepared by the European Centre for Medium-Range Weather Forecasting (ECMWF) [*Bengtsson*, 1985; *Hollingsworth et al.*, 1986]. The various meteorological parameters were available twice daily (0000 and 1200 UTC) at a horizontal resolution of 2.5° longitude by 2.5° latitude at 13 isobaric levels (1000, 925, 850, 700, 500, 400, 300, 250, 200, 150, 100, 70, and 50 hPa). Our computational domain was 75°S to 25°N and 75°W westward to 60°W.

Kinematic backward trajectory analysis was employed to determine likely source regions and transport paths of air parcels sampled during the PEM-T flights. The kinematic scheme uses only the horizontal and vertical wind components to track air parcels [*Draxler*, 1991; *Doty and Perkey*, 1993; *Krishnamurti et al.*, 1993; *Garstang et al.*, 1996]. There are no "explicit assumptions" about the flow field, for example, the isentropic assumption. Additional details about the trajectory model are given by *Fuelberg et al.* [1999]. Kinematic trajectories are compared with their isentropic counterparts by *Fuelberg et al.* [1996b].

All trajectories are subject to limitations due to data availability and numerical procedures. The relatively coarse spatial and temporal resolution of the ECMWF data does not resolve small, short-lived mesoscale phenomena. For example, winds associated with individual convective elements are not adequately resolved, although composite effects of the convective elements are included. In addition, since the Pacific Basin is a relatively data sparse region, meteorological features are less accurately placed than over data rich areas. Although the ECMWF vertical motions needed to calculate our kinematic trajectories probably are the least reliable of the various meteorological parameters, all of the parameters are dynamically consistent with each other. In addition, *Stohl et al.* [1995] have noted that the temporal, horizontal, and vertical interpolations required by the kinematic scheme are a source of uncertainty. These various data and numerical limitations produce trajectories whose accuracy deteriorates with increasing time. Nonetheless, both kinematic and isentropic trajectories of 7 days duration or longer are relatively common in the literature, for example, *Fuelberg et al.* [1999] (10 days), *Rood et al.* [1997] (7 days), *Garstang et al.* [1996] (10 days), *Swap et al.* [1996] (10 days), *Thompson et al.* [1996] (10 days).

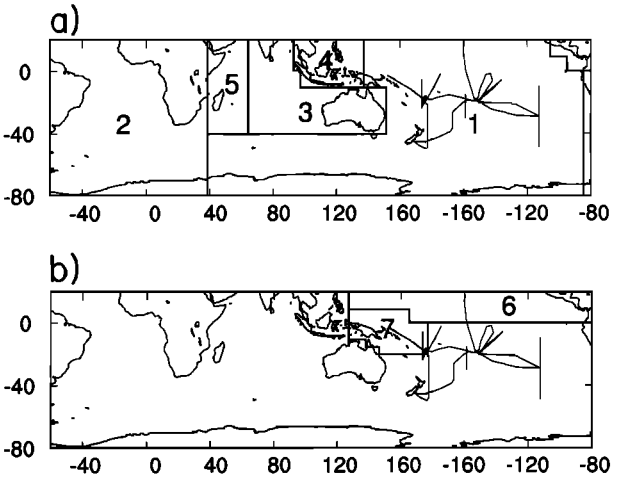

Figure 2. (a) Source regions of trajectory clusters in the nonconvective categories: (1) aged marine, (2) long-range, (3) Australia, (4) Australia/Southeast Asia, and (5) not classified. (b) Source regions of trajectory clusters in the convective category: (6) ITCZ and (7) SPCZ. Flight tracks for the DC-8 during PEM-T that were used in the current study are superimposed. Only those flight segments north of 35°S were investigated.

Arrival locations of our 10-day backward trajectories were chosen along the flight tracks (Figure 2) at intervals of 2.5°. Additional trajectories were calculated in areas of significant aircraft altitude change (>1000 feet). Arrival times were either 0000 or 1200 UTC on each flight day, that is, the time closest to the flight. Since the reliability of individual trajectories is affected by the erroneous placement of meteorological features and by horizontal and vertical wind shear, we employed a "clustering technique" [e.g., *Merrill et al.*, 1985; *Fuelberg et al.*, 1996a]. That is, at each trajectory arrival location along the flight track, we superimposed a 4° × 4° square to create four additional arrival points. Thus each cluster consisted of five trajectories, one at the center of the square (the original flight track point) and four new points at the corners. We did not consider flight locations within the MBL because backward trajectories arriving at such low altitudes generally terminate at the surface before the end of 10 days.

2.2. Data Groups

A series of tests assessed the reliability of the trajectories, that is, whether they could be used confidently to describe origins of the various chemical samples. The first test considered horizontal wind shear. Specifically, at least three of the five trajectories comprising a cluster were required to have a consistent geographical origin. That is, at least three trajectories must have originated within one of the five regions that are shown in Figure 2a and described in later paragraphs. If this requirement was not met, the point was excluded from further consideration.

Test two was used to distinguish between two major categories of trajectories: nonconvective and convective. For the nonconvective category, at least three of five trajectories passing the common origin test had to experience changes in potential temperature (theta) <8°C within each 24 hour period. Comparisons between trajectory paths and satellite imagery show that the 8°C threshold does not remove all encounters with convection. However, the convective exposure of trajectories

in this category is not widespread or long lasting. For the convective category, at least three out of five trajectories passing the common origin test must have experienced >10°C change in theta within a 24-hour period. In addition, of those that experienced the >10°C theta change, at least three must have passed through extensive satellite-observed convection on the day that the large diabatic change occurred.

The final check required trajectories to remain within the data domain for at least 5 days. Those traveling outside the domain between days 5 and 10 were retained only if their geographical category at that time was clearly known. This situation usually occurred when parcels reached the western border of the domain (60°W, near South America) between days 5 and 10.

Upon completing these checks, the remaining clusters had at least three out of five trajectories that passed both the theta and geographical origin tests and did not terminate within 5 days of arriving at the flight track. A total of 133 out of the original 367 clusters arriving between 0° and 35°S remained in the nonconvection category. Similarly, the convective category consisted of 18 clusters. Although this is a major reduction in sample size, we believe these trajectories can be used with confidence to determine the origins of air parcels sampled by the DC-8. The representativeness of this final data set is described in section 2.3.

Trajectory clusters passing the quality control tests were classified according to their source region and transport path. We used four categories for clusters not encountering widespread, significant convection, and two categories for clusters that did experience such convection (Figure 2). The aged marine trajectories (labeled 1 in Figure 2a) originated over the Pacific Ocean and remained over water (east of 40°E) during the entire 10-day calculation period. Long-range trajectories (labeled 2) originated west of 40°E and tracked eastward toward the Pacific Basin. Most of these trajectories traveled over southern Africa and/or South America. The Australian category (labeled 3) includes trajectories, which traveled over Australia during the 10-day period. However, they did not travel over any other land mass and did not extend west of 65°E. The fourth category represents trajectories which traveled over Southeast Asia before passing over Australia and then into the Pacific Basin. Trajectories originating in region 5 were not classified so there would be a clear distinction between categories 2 and 3.

The convective group consisted of two categories (Figure 2b), one representing parcels experiencing extensive convection near the ITCZ (labeled 6), and the other for parcels influenced by widespread convection near the SPCZ (labeled 7).

2.3. Chemical Data

Our chemical data set links the measured chemical data with the kinematic backward trajectories. It was prepared at Harvard University from archived files submitted by the DC-8 principal investigators to the PEM-T project office. These archived files are public domain at the web site http://www-gte.larc.nasa.gov. The archived files identify the responsible investigator, the instrumental technique, and the instrument performance characteristics. Specifically, the merged data set was a 5 min average of the chemical data centered on each trajectory arrival location along the flight track. As noted earlier, most of these locations were at intervals of 2.5°. In some cases, averages less than 5 min were required to avoid time overlaps. When a chemical measurement was below the level of detection (LOD, values of *Hoell et al.* [1999]), we substituted that value for the measured one. LOD values are underlined in the tables of chemical concentrations that follow to identify their contributions to the analyses.

Table 1 describes the representativeness of our data set as a function of altitude. Specifically, the values from *Schultz et al.* [1999] are medians of all PEM-T measurements between 0° and 35°S. Except for the less frequent hydrocarbon samples, these values were obtained from a merged data set at 1 min intervals. The other two columns in each altitude range denote medians for our original 367 trajectory locations and final set of 133 locations. As stated above, these values represent 5 min averages centered at each trajectory location. The statistics show that most trajectories passing the various checks described earlier (Trj2) arrive at the flight tracks in the middle and upper troposphere. The corresponding chemical data closely represent the complete PEM-T population in most cases.

Various atmospheric chemical species can be used to determine origins of air samples and the influences of atmospheric processes such as convection and mixing. In general, one must examine a number of species in order to represent and understand the chemical signature of tropospheric air in remote regions. Such air may have a mixed origin and may have been processed, either photochemically or by mixing, at various times. Although we have examined all species measured onboard the DC-8, the following discussions are limited to those species which we believe are most informative for the issues being considered.

Ozone concentrations [*Gregory et al.*, 1996, 1999; *Talbot et al.*, 1994, 1996a, b, 1997] typically are greatest in stratospherically influenced air (>120 ppbv), are enhanced in plumes originating from land sources (70–100 ppbv), are relatively small (40–60 ppbv) in clean air, usually are small in MBL air (20 to 30 ppbv), and can be very small (<10 ppbv) in MBL air at selected tropical locations (e.g., within the ITCZ). The concentration of carbon monoxide (CO) also is a reliable indicator of air mass history [*Harriss et al.*, 1992]. Relatively small values (less than 60 ppbv) indicate either stratospherically influenced air or well-aged tropospheric air [*Talbot et al.*, 1996b]. CO mixing ratios near 50 ppbv characterized relatively clean air in the southern hemisphere during PEM-T [*Gregory et al.*, 1999]. CO mixing ratios exceeding 80 ppbv in the middle and upper troposphere suggest a continental influence. Perchloroethene (C_2Cl_4) and other fluorocarbon species are useful for determining whether CO is from biomass burning or urban emissions [*Gregory et al.*, 1996]. Formic acid (HCOOH) and acetic acid (CH_3COOH) exhibit large mixing ratios in biomass burning impacted air [*Talbot et al.*, 1990] and serve as positive tracers for this source of pollution. However, since these species are relatively soluble, they can be depleted by moist convective processes.

Ratios of hydrocarbon concentrations (e.g., C_2H_2, C_2H_6, C_3H_8) to CO and among themselves depend on photochemical lifetimes and thus provide information about transport times from emission sources. However, one must note that (1) the photochemical lifetimes of most chemical species are altitude dependent and (2) that mixing (or other atmospheric processing) during transport also influences these ratios [*McKeen and Liu*, 1993; *McKeen et al.*, 1996]. We calculated many hydrocarbon ratios during the analyses; however, only the ratio ethyne (acetylene) to CO (C_2H_2/CO) will be used in later discussions. This ratio is informative because both C_2H_2 and CO generally

Table 1. Median Concentrations of Chemical Species Observed Between 0° and 35°S During PEM-Tropics A

	0–2 km			2–4 km			4–8 km			8–12 km		
Species	Schtz	Trj1	Trj2	Schtz	Trj1	Trj2	Schtz	Trj1	Trj2	Schtz	Trj1	Trj2
N	...	72	4	...	41	23	...	113	58	...	141	48
O_3	26	25	33	44	41	38	47	48	47	40	41	47
CO	58	60	63	63	61	60	60	61	59	60	60	61
C_2H_2	43	41	50	58	58	37	51	48	47	44	43	53
PAN	(1)	(1)	2	10	9	2	52	57	51	40	40	50
NO	1	1	3	5	6	6	12	13	11	42	40	53
NO_x	4	5	8	15	25	25	25	22	17	70	50	68
HNO_3	19	20	71	77	86	81	75	74	72	54	56	86
HCOOH	23	28	84	50	52	46	46	48	46	47	50	57
CH_3COOH	25	28	58	51	45	44	46	54	53	44	45	51
H_2O_2	1081	1213	1744	1091	1241	1311	585	601	629	209	197	162
CH_3OOH	952	950	903	544	580	641	299	293	301	119	99	68
CH_3I	0.37	0.37	0.19	0.10	0.08	0.08	0.06	0.06	0.06	0.06	0.06	0.07
$CHBr_3$	1.0	1.0	0.7	0.6	0.6	0.6	0.5	0.5	0.4	0.3	0.3	0.4
^7Be	188	(100)	...	287	220	215	388	302	318	504	347	462
^{210}Pb	1.7	1.8	...	2.2	2.9	3.8	2.6	2.4	2.8	2.2	2.1	4.2
$RelHum_w$	82	83	45	21	23	23	18	14	13	14	14	23

Values from *Schultz et al.* [1999] (denoted Schtz) represent the complete data set, while those in Trj1 and Trj2 represent values for our original set of 367 trajectory clusters and final set of 133 clusters. Mixing ratios are given in parts per trillion by volume (pptv), except for CO and O_3 which are in parts per billion by volume (ppbv), ^7Be and ^{210}Pb which are in fCi/scm, and relative humidity with respect to water (%). LOD values are in parentheses. N is the number of trajectory clusters in each altitude interval.

have a common combustion source but differing lifetimes [*Gregory et al.*, 1999]. The lifetime of CO typically is of the order of months, whereas the lifetime of C_2H_2 is 1 to 2 weeks [*Talbot et al.*, 1996b]. Values of the ratio decrease with increased photochemical aging [e.g., *Greenberg and Zimmerman*, 1984; *Greenberg et al.*, 1990; *Singh and Zimmerman*, 1992; *Gregory et al.*, 1999]. For our applications a ratio of ~2 (pptv/ppbv) represents air that is aged 2–3 days from its source region, while a value of ~0.5 represents air that is approximately 10 days aged [*Smyth et al.*, 1996].

Nitrogen compounds and their ratios provide additional information about air parcel history and the extent of air parcel processing. The sum of NO, NO_2, peroxyacetyl nitrate (PAN), and nitric acid (HNO_3), hereafter denoted ΣNO_t, typically is elevated within urban and biomass burning impacted air. NO is the emitted form of nitrogen that rapidly attains a photochemical steady state with NO_2. PAN and HNO_3 are secondary products of pollution; high concentrations indicate that the air was subjected to urban or biomass burning emissions [e.g., *Talbot et al.*, 1994, 1996b]. HNO_3 also can have a stratospheric origin. HNO_3 and PAN are the principal storage species for nitrogen oxides. HNO_3 is slowly recycled to NO_2 by photochemistry or is removed rapidly from the atmosphere by particle surfaces or by precipitation. PAN is stable at cold temperatures and can be transported long distances in the middle to upper troposphere [*Singh et al.*, 1990; *Ridley et al.*, 1990]. It experiences rapid thermal decomposition within warm air and generates NO_2 and subsequently HNO_3. Large ratios of NO_x to ΣNO_t, where $NO_x \equiv NO + NO_2$, indicate recent emissions of nitrogen oxides. They also may indicate recent rapid warming or physical removal of HNO_3. Possible sources of NO pertinent to PEM-T include lightning [*Ehhalt et al.*, 1992] as well as combustion and stratospheric inputs [*Liu et al.*, 1996].

Chemical tracers of convection, particularly marine convection, include methyl iodide (CH_3I), methyl bromoform ($CHBr_3$), "depleted" O_3, and methyl hydroperoxide (CH_3OOH) [*Cohan et al.*, 1999]. CH_3I and $CHBr_3$ are emitted from seawater, exhibiting large concentrations in the MBL. Since CH_3I also is produced by biomass burning, enhanced concentrations by themselves do not imply marine convection [*Andreae et al.*, 1996]. The typical lifetime of CH_3I in the tropics is 4 days, while the lifetime of $CHBr_3$ is longer. The lifetime of CH_3OOH is 1–2 days. O_3 is photochemically destroyed in the MBL [e.g., *Kawa and Pearson*, 1989; *Heikes et al.*, 1996b]. The lifetime of "depleted" O_3 depends on NO_x, ranging from a week to months [*Liu et al.*, 1987]. Hydrogen peroxide (H_2O_2) also can be a tracer of convection [*Heikes*, 1992; *Heikes et al.*, 1996a; *Pickering et al.*, 1996; *Cohan et al.*, 1999]. Both H_2O_2 and CH_3OOH exhibit maxima in the lower troposphere; H_2O_2 near the MBL. Once transported aloft, CH_3OOH decays to background values within 1–2 days, whereas H_2O_2 does not decrease significantly during the first several days following convection [*Jaeglé et al.*, 1997; *Cohan et al.*, 1999]. However, H_2O_2 can be removed by precipitation or by reactions in cloud water during transport. Therefore caution should be exercised when using it as a tracer. Chemical steady state concentrations of H_2O_2 generally are greater than those for CH_3OOH. Therefore it has been argued that the ratio $H_2O_2/CH_3OOH < 1$ indicates air parcels influenced by recent convection and precipitation [*Heikes*, 1992; *Heikes et al.*, 1996a; *Pickering et al.*, 1996; *Cohan et al.*, 1999]. The effectiveness of CH_3OOH, H_2O_2, and the ratio H_2O_2 to CH_3OOH as tracers of convection decreases with time due to photochemistry and mixing. Other water soluble species such as CH_3COOH, HCOOH, and HNO_3 are useful for assessing whether air parcels were convectively influenced. Small values in the upper troposphere may indicate surface layer air which has been depleted of these species by surface removal or by precipitation scavenging during convection [*Talbot et al.*, 1996a].

Particle-borne species such as beryllium 7 (^7Be) and lead 210 (^{210}Pb) also help identify parcels influenced by convection and particle scavenging processes. Beryllium 7 is produced in the upper troposphere and stratosphere by cosmic rays and is then absorbed on particles. It has been used as a tracer for stratospheric air in the troposphere [*Bhandari et al.*, 1966; *Elbern et al.*, 1997; *Dibb et al.*, 1996, this issue]. Lead 210 is a product of

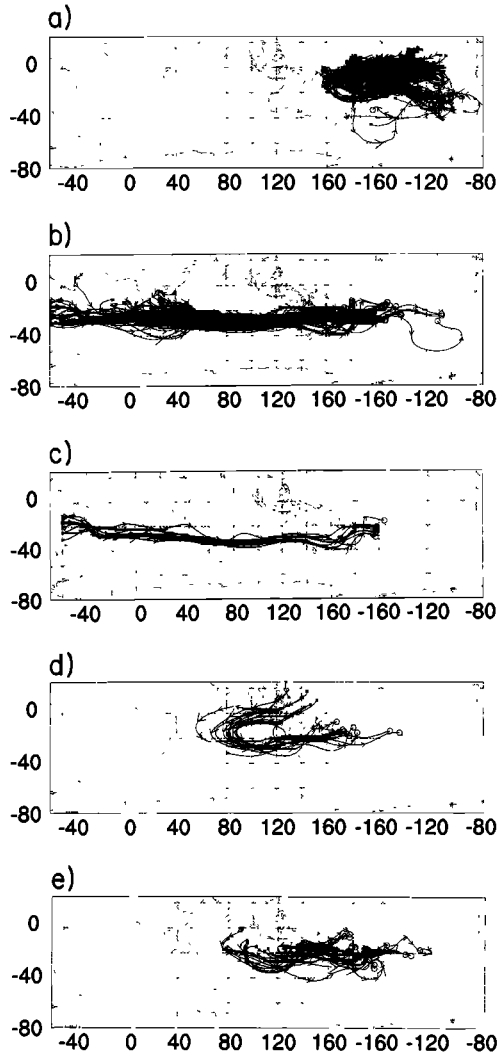

Figure 3. Trajectory paths of the four nonconvective categories: (a) aged marine, (b) long-range, (c) only those trajectories of the long-range category reaching South America, (d) Australia/Southeast Asia, and (e) Australia. For the sake of clarity, only one representative trajectory from each cluster has been plotted.

radon decay and also is absorbed on particles. Concentrations of ^{210}Pb generally are large in the boundary layer. This air can be transported aloft by dry convection, with the recently uplifted air having large concentrations of ^{210}Pb and other boundary layer tracers. Thus radon and its daughter ^{210}Pb have been used as tracers for continental air [*Kritz et al.*, 1991; *Dibb et al.*, this issue]. Both ^{7}Be and ^{210}Pb are removed from the air by particle removal processes (e.g., sedimentation and precipitation) that primarily occur in the lower troposphere [e.g., *Turekian et al.*, 1989; R. Arimoto et al., manuscript in preparation, 1999]. Large concentrations of ^{7}Be indicate air that has been in the upper troposphere for a long period of time and has been free of particle removal processes. Large concentrations of ^{210}Pb in the upper troposphere indicate air which once was in contact with the continents, but which has been aloft for a long period and free from particle removal processes. Convective outflow of low-altitude air having undergone particle scavenging is expected to be depleted in these elements.

3. Characteristics of Aged Marine Air

The sixty-six 10-day backward trajectory clusters comprising the aged marine category are shown in Figure 3a. These clusters represent 12 different flights. Figure 4a shows trajectory altitudes as a function of time, while Table 2 gives corresponding statistics. Median values will be cited in the text, generally without stating the word "median." The arrival altitude along the DC-8 track is 6.5 km, while altitudes 5 and 10 days prior to arrival are 6.9 and 7.4 km, respectively. Although altitudes of individual trajectories show only moderate variations (Figure 4a), their arrival altitudes do vary considerably, reflecting the altitude range of the DC-8 flight tracks. Thus the term "aged marine air" does not simply denote parcels near the ocean surface, but includes parcels arriving at all altitudes that have remained over water during the entire 10-day period. This is an important distinction since concentrations of chemical species such as H_2O_2 and CH_3OOH exhibit an altitude dependency [e.g., *Cohan et al.*, 1999]. Most of these trajectories remain in the tropical latitudes (Figure 4a) where relatively slow wind speeds (~8 m s^{-1}) produce short trajectory paths (~7000 km). Some trajectories show flow reversals or are circular during their 10-day histories.

Chemical characteristics (Table 3) of the aged marine parcels indicate, as expected, relatively aged, clean air. The small ratio of C_2H_2/CO (0.56 pptv/ppbv) is consistent with the trajectory classification of air aged at least 10 days from continental source regions [e.g., *Greenberg and Zimmerman*, 1984; *Greenberg et al.*, 1990; *Singh and Zimmerman*, 1992; *Gregory et al.*, 1999]. The parcels have small median mixing ratios of O_3 (34 ppbv), CO (56 ppbv), PAN (16 pptv), and HNO_3 (52 pptv). The ratio $NO_x/\Sigma NO_i$ is <0.1. One should note that since the ratio $NO_x/\Sigma NO_i$ requires concurrent measurements of NO, NO_2, HNO_3, and PAN, the number of samples comprising the ratio (N in the tables) generally is less than numbers of the other nitrogen species. The ratio value suggests that the air parcels have not received fresh injections of emissions from lightning, jet aircraft, or industrial sources. Current results are consistent with other studies of Pacific aged marine air [e.g., *Talbot et al.*, 1996b, 1997], noting the 5-day over-the-ocean classification in Talbot's studies as opposed to our 10 days. These contrasting definitions do not warrant a rigorous comparison of values; rather, the reader is referred to these references.

4. Characteristics of Long-Range Air

Thirty-nine long-range trajectory clusters representing 10 different flights originate west of 40°E (Figure 3b). Trajectories within this long-range category arrive at the flight tracks at a median latitude of 21.8°S (Table 2), farther south than the aged marine category (12.8°S). Thus they are influenced by the relatively strong prevailing westerlies (Figure 1b). Their arrival altitude (10.2 km, Table 2) is significantly higher than trajectories of the aged marine category (6.5 km). These long-range trajectories pass over the east coast of Australia (155°E) approximately 1.9 days prior to reaching the DC-8 track (Table 2) and most pass over, or just south of the east coast of Africa (40°E) ~5.5 days prior to arriving at the flight track. This corresponds to a median speed of 30 m s^{-1}. Trajectories from nine clusters in the long-range nonconvective category extend to the east coast of South America (north of 25°S) within 10 days of arriving at the flight track (also depicted separately in Figure 3c). The trajectories undergo weak subsidence in route

to the Pacific Basin (Figure 4b). Additional statistics about the trajectories are given in Table 2.

Median mixing ratios of O_3 (82 ppbv), CO (70 ppbv), PAN (105 pptv), and HNO_3 (145 pptv) (Table 4) are greater than those of the aged marine air (Table 3). Mixing ratios of NO and NO_x (65 pptv and 87 pptv) also are greater than the aged marine values, as is the ratio $NO_x/\Sigma NO_i$ (0.20 versus 0.09). The median ^{210}Pb value is enhanced compared to aged marine air (4.7 versus 2.2 fCi/scm) indicating a continental influence, consistent with the other species. However, values of C_2Cl_4 (as well as the other fluorocarbons) are similar to those of aged marine air, suggesting that any continental influence is not of urban or industrial origin. HCOOH and CH_3COOH also are enhanced with respect to the aged marine air, supporting an impact from biomass burning on the long-range group. Median values of C_2Cl_4 (not shown) range from ~1 to 1.5 pptv among all the nonconvective and convective categories, and no significant differences are observed for any of the fluorocarbons

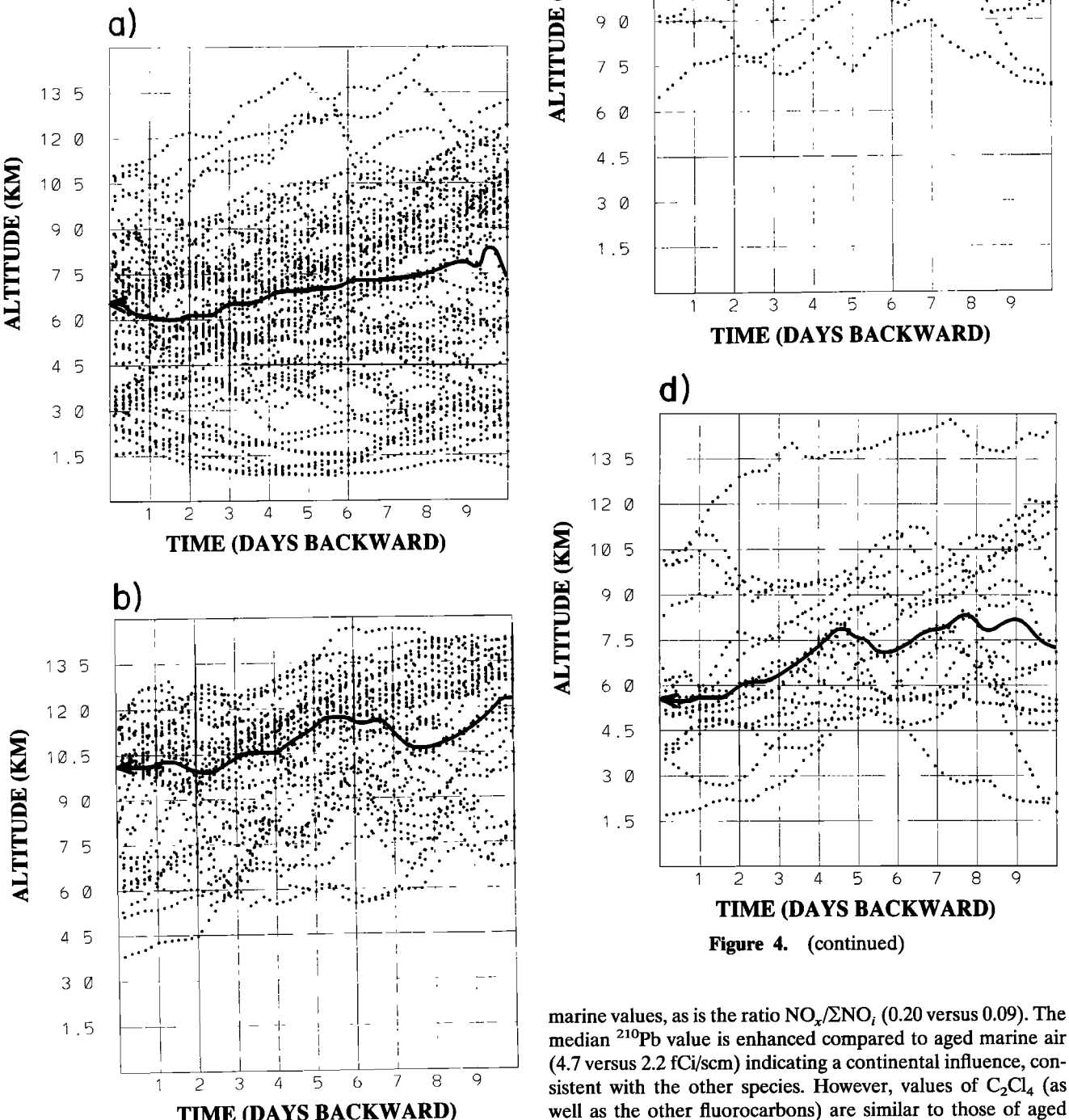

Figure 4. Time series of altitude for trajectories in the four nonconvective categories: (a) aged marine, (b) long-range, (c) Australia/Southeast Asia, (d) Australia, and (e) the convective category. For the sake of clarity, only one representative trajectory from each cluster has been plotted. The bold line on each panel denotes median altitudes at each time. Trajectories arrive at the DC-8 flight track on day 0.

Figure 4. (continued)

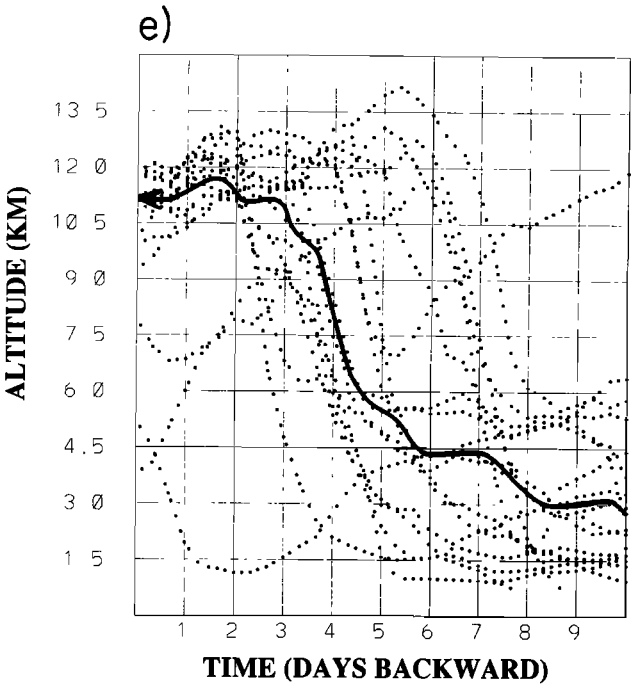

Figure 4. (continued)

among any of the categories. Therefore we conclude that urban, industrial emissions are not a significant factor when considering continental influences during PEM-T. As discussed in some detail in the PEM-T special section of the *Journal of Geophysical Research* (1999), air within the South Pacific Basin was heavily impacted by seasonal biomass burning. The data in Table 4 are consistent with biomass burning.

The median mixing ratio of ^{7}Be (1000 fCi/scm, Table 4) is considerably greater than in any other category. The range of individual values (not shown) is similar to those reported by *Dibb et al.* [this issue] for remote Pacific air. An examination of the individual samples does not suggest an obvious stratospheric origin; for example, the greatest O_3 value is only 128 ppbv, and corresponding peak values of potential vorticity along the trajectories do not exceed the commonly accepted stratospheric threshold. The large values of ^{7}Be may have been produced in air remaining just below the tropopause for a

Table 2. Trajectory Data for Air Parcels

	Median Altitude, km	Median Latitude, °S	Median Time, days
Nonconvective			
Aged marine			
Arrival	6.5	12.8	···
5 days	6.9	7.1	···
10 days	7.4	3.5	···
Long-range			
Arrival	10.2	21.8	···
Eastern Australia	10.1	26.2	1.9
Eastern Africa	11.2	26.6	5.5
Northern South America*	10.1	19.9	7.2
Southeast Asia			
Arrival	10.0	14.5	···
Eastern Australia	11.6	18.7	1.6
Southeast Asia	13.1	7.3	6.0
Australia			
Arrival	5.5	19.3	···
Eastern Australia	7.4	20.4	4.8
Convective			
Arrival	11.2	6.8	···
5 days	5.7	4.1	···
10 days	2.8	0.6	···

*Most long-range trajectories did not extend back to South America during the 10-day period. Nine of the 39 trajectories did reach South America north of 29°S; their statistics are given.

Table 3. Chemical Characteristics of Principle Species for 66 Aged Marine Trajectory Clusters Representing 12 Different Flights

Species	LoQuart	Median	UpQuart	N
O_3	27	34	45	66
CO	52	56	60	64
C_2H_2	22	30	41	54
C_2H_2/CO	0.42	0.56	0.70	53
PAN	7	16	43	60
NO	4	7	12	47
NO_x	8	10	18	25
HNO_3	28	52	75	57
$NO_x/\Sigma NO_i$	0.08	0.09	0.14	13
HCOOH	20	37	52	53
CH_3COOH	26	37	53	54
H_2O_2	462	701	1146	67
CH_3OOH	292	388	616	63
H_2O_2/CH_3OOH	1.6	1.9	2.6	63
CH_3I	0.05	0.08	0.12	55
$CHBr_3$	0.43	0.56	0.66	55
^{7}Be	(100)	220	318	44
^{210}Pb	1.6	2.2	3.3	40
$RelHum_w$	15	28	55	66

Mixing ratios for chemicals are given in parts per trillion by volume (pptv); except for CO and O_3 which are in parts per billion by volume (ppbv), ^{7}Be and ^{210}Pb which are in fCi/scm, and relative humidity with respect to water (%). LOD values are in parentheses to indicate their contributions.

Table 4. Chemical Characteristics of Principle Species for 39 Long-Range Trajectory Clusters Representing 10 Different Flights

Species	LoQuart	Median	UpQuart	N
O_3	67	82	87	39
CO	60	70	84	36
C_2H_2	54	71	107	38
C_2H_2/CO	0.8	1.1	1.3	35
PAN	78	105	186	33
NO	41	65	88	29
NO_x	53	87	113	18
HNO_3	103	145	189	34
$NO_x/\Sigma NO_i$	0.12	0.20	0.33	18
HCOOH	58	97	186	34
CH_3COOH	42	86	141	34
H_2O_2	91	154	274	34
CH_3OOH	(25)	38	145	26
H_2O_2/CH_3OOH	2.1	3.4	4.3	26
CH_3I	0.03	0.04	0.06	38
$CHBr_3$	0.09	0.17	0.32	34
^{7}Be	432	1000	1243	26
^{210}Pb	3.7	4.7	6.2	20
$RelHum_w$	3	8	15	36

Mixing ratios for chemicals are given in parts per trillion by volume (pptv); except for CO and O_3 which are in parts per billion by volume (ppbv), ^{7}Be and ^{210}Pb which are in fCi/scm, and relative humidity with respect to water (%). LOD values are in parentheses to indicate their contributions.

week or more, if that air avoided precipitating clouds. The high altitudes traveled by many of these trajectories en route to the DC-8 sampling sites (Figure 4b), together with satellite imagery, suggest that the parcels are above most clouds even in regions of relatively strong convection, hence scavenging is inefficient. Furthermore, the submicron size aerosols on which ^{7}Be is absorbed have small settling velocities, causing dry deposition to be relatively small. As a result, concentrations of ^{7}Be will increase. Another possible mechanism producing large ^{7}Be is that air at such high altitudes likely experiences a stratospheric influence. Specifically, even outside of tropopause folding, there is some diffusive transport of tracers across the tropopause, with just small amounts of stratospheric air delivering large amounts of ^{7}Be to the troposphere. Ongoing analyses of ^{10}Be will provide additional information about this issue.

The ratio C_2H_2/CO for the long-range trajectories is 1.1 pptv/ppbv. Point model simulations of *Schultz et al.* [1999] indicate that the lifetime of CO near 20°S ranges from 29 to 64 days, depending on altitude, whereas the corresponding lifetime for C_2H_2 is 10 to 26 days. The current ratio indicates that parcels probably were most influenced by combustion sources 5–7 days prior to reaching the flight track [*Greenberg and Zimmerman*, 1984; *Greenberg et al.*, 1990; *Singh and Zimmerman*, 1992; *Gregory et al.*, 1999]. This timing is more consistent with trajectory passage over Africa (~5.5 days) than over Australia (2 to 3 days). *Blake et al.* [1996] found that the ratio C_2H_2/CO was 3–4 for fresh emissions over southern Africa.

Regions over Africa between 5° and 25°S normally experience extensive biomass burning during the September time period [e.g., *Justice et al.*, 1996]. During PEM-T there were more fires along the South African coast than normal (south of ~22°S), and fewer fires near Angola and Zambia [*Olson et al.*, 1999]. Satellite imagery (not shown) indicates considerable deep convection over central Africa (generally between 0° and 10°S) during the study period, but much less convection over southern Africa (between 10° and 30°S). Thus most of the convection was somewhat north of the major trajectory paths (Figure 3b). Nonetheless, the chemical data in Table 4 suggest that by-products of biomass burning were carried aloft by convection [e.g., *Pickering et al.*, 1996] and then transported eastward to the DC-8 measurement sites. That convection was not sufficiently widespread or long lasting to produce the large diabatic rates that would have removed these trajectories from the nonconvection group.

We believe that Australian sources did not greatly influence these long-range parcels. There was less burning over Australia than over southern Africa [*Olson et al.*, 1999; European Space Agency, 1998]. Furthermore, the trajectories passed over Australia only 2–3 days prior to arrival and were at relatively high altitudes (~10 km). Satellite imagery indicates that very little convection over Australia reaches the altitudes of the trajectories over the continent. Instead, satellite-derived cloud-top temperatures of 230–250 K correspond to cloud tops of 7–8 km, considerably below the median trajectory altitude at the east coast. These tops generally are lower than those of deep tropical convection (11–14 km) over the Pacific Basin.

As noted earlier and shown in Figure 3c, trajectories from nine clusters in the long-range category extend to the east coast of South America (north of 25°S) within 10 days of arriving at the flight track. Eight of these very long-range trajectory clusters arrive at DC-8 flight 12 on September 19, 1996. It is informative to examine characteristics of these clusters in detail. They pass over Australia approximately 2 days before arriving at the flight track, over southern Africa ~4.5 days before arrival, and extend to South America ~7 days prior to arriving at the flight track. This corresponds to a median speed of 36 m s^{-1}. The trajectories remain at high altitudes (~10.5 km) throughout their transits.

Table 5. Chemical Characteristics of Principle Species for Nine Trajectory Clusters Within the South American Case of the Long-Range Category

Species	LoQuart	Median	UpQuart	N
O_3	83	89	101	9
CO	68	108	138	8
C_2H_2	69	124	262	9
C_2H_2/CO	1.3	1.5	1.9	8
PAN	102	193	310	9
NO	51	65	70	9
NO_x	85	87	101	9
HNO_3	134	226	304	9
$NO_x/\Sigma NO_i$	0.12	0.13	0.23	9
HCOOH	142	284	589	9
CH_3COOH	88	110	177	9
H_2O_2	98	255	387	9
CH_3OOH	25	25	44	7
H_2O_2/CH_3OOH	3.4	4.4	6.0	7
CH_3I	0.02	0.03	0.03	9
$CHBr_3$	0.08	0.10	0.18	9
^{7}Be	134	445	445	7
^{210}Pb	6.0	8.1	9.5	6
$RelHum_w$	3	4	7	9

One flight is represented. Mixing ratios for chemicals are given in parts per trillion by volume (pptv), except for CO and O_3 which are in parts per billion by volume (ppbv), ^{7}Be and ^{210}Pb which are in fCi/scm, and relative humidity with respect to water (%). LOD values are in parentheses to indicate their contributions.

Chemical data for the nine trajectory clusters reaching northern South America (Table 5) exhibit enhanced values (compared to entire long-range category) of O_3 (89 ppbv), CO (108 ppbv), HNO_3 (226 pptv), PAN (193 pptv), HCOOH (284 pptv), and ^{210}Pb (8.1 fCi/scm). The C_2H_2/CO ratio (1.5 pptv/ppbv) is greater than that of the complete long-range category (1.1 pptv/ppbv), corresponding to a shorter processing time from the source region. Median mixing ratios of NO and NO_x are 65 and 87 pptv, respectively, similar to those for the complete long-range category. The ratio $NO_x/\Sigma NO_i$ is smaller (0.13) than that of the complete long-range group.

Some of the long-range trajectories that did not reach South America within 10 days might have done so if the calculation period were longer. Thus the enhanced chemical signature for trajectories reaching South America may be due, in part at least, to the more recent injection of biomass burning emissions over South America (~7 days compared to 10+ days). These parcels also pass over Africa approximately 1 day earlier than parcels in the composite long-range group (~4.5 days versus ~5.5 days). Much of northern South America experienced extensive biomass burning during PEM-T (European Space Agency, 1998). Furthermore, GOES-8 satellite imagery indicates widespread deep convection over northern South America (north of ~20°S) on most afternoons during PEM-T. Since this convection generally is not persistent on any given day, potential temperatures of the trajectories were not sufficiently affected to remove them from the nonconvective group. Satellite-derived cloud-top temperatures of the deepest convection generally are between 200 and 230 K, corresponding to heights of 11–14 km. Therefore it appears that biomass burn-

Table 6. Chemical Characteristics of Principle Species for 11 Australia/Southeast Asian Trajectory Clusters Representing Four Different Flights

Species	LoQuart	Median	UpQuart	N
O_3	43	46	46	11
CO	66	67	68	11
C_2H_2	63	73	75	8
C_2H_2/CO	1.0	1.1	1.1	8
PAN	30	38	48	9
NO	37	50	89	9
NO_x	40	51	80	7
HNO_3	40	51	71	10
$NO_x/\Sigma NO_i$	0.26	0.34	0.38	4
HCOOH	33	41	58	9
CH_3COOH	21	27	45	9
H_2O_2	118	162	205	11
CH_3OOH	91	99	169	7
H_2O_2/CH_3OOH	1.0	2.7	3.5	7
CH_3I	0.04	0.06	0.06	8
$CHBr_3$	0.10	0.20	0.37	7
^7Be	110	302	462	10
^{210}Pb	2.1	3.3	4.8	9
$RelHum_w$	6	7	15	11

Mixing ratios for chemicals are given in parts per trillion by volume (pptv), except for CO and O_3 which are in parts per billion by volume (ppbv), ^7Be and ^{210}Pb which are in fCi/scm, and relative humidity with respect to water (%). LOD values are in parentheses to indicate their contributions.

ing by-products were lofted into the upper troposphere by the convection. This process has been discussed by *Pickering et al.* [1990, 1991, 1992, 1996].

5. Characteristics of Australia/Southeast Asian Air

The 11 trajectory clusters comprising the Australia/Southeast Asian category (Figure 3d) pass over Australia and the islands of Southeast Asia (e.g., Indonesia, Malaysia, Philippines) within 10 days of arriving at the DC-8's location. These trajectories, representing four different flights, arrive along the flight tracks at a median altitude of 10.0 km (Table 2) and typically travel at high altitudes (9–15 km, Figure 4c) throughout their 10-day periods. They arrive at the flight track farther north (14.5°S) than the long-range trajectories (21.8°S).

The Southeast Asian trajectories pass over the east coast of Australia ~1.6 days prior to reaching the flight tracks (Table 2), slightly sooner than the long-range trajectories (~1.9 days). Their total travel distance is ~18,500 km, compared to 27,000 km for the long-range trajectories. The Southeast Asian trajectories traverse the east coast of Australia at somewhat higher altitudes (11.6 km) than those in the long-range category (10.1 km), while their latitude over eastern Australia (18.7°S) is farther north than the long-range trajectories (26.2°S). The Southeast Asian trajectories transit the boundary between the prevailing westerlies and tropical easterlies. Thus they swing around the western side of the middle tropospheric subtropical anticyclone (Figure 1b).

Chemical characteristics of the Australian/Southeast Asian clusters (Table 6) indicate a weak combustion signature. Median values are O_3 (46 ppbv), CO (67 ppbv), HNO_3 (51 pptv), PAN (38 pptv), NO (50 pptv), and NO_x (51 pptv). The C_2H_2/CO ratio (1.1 pptv/ppbv) is the same as that of the long-range trajectories, suggesting that parcels receive their combustion influence approximately 5–7 days prior to arriving at the flight track. The trajectories pass over Southeast Asia ~6 days prior to arrival, agreeing with the combustion influence time suggested by the chemistry. Since they pass over Australia ~1.6 days back, Australian sources probably had little influence on the chemistry of these parcels. Also, as noted previously, most convective cloud tops over Australia were only 7–8 km. Thus any by-products of burning probably did not reach the altitude of the trajectories over Australia (~11.6 km). However, the Australian/Southeast Asian air does exhibit a greater $NO_x/\Sigma NO_i$ ratio (0.34) than the long-range category. This may indicate some influence of Australian emissions or, more probably, the effects of lightning over Southeast Asia. Lightning plots given by *Fuelberg et al.* [1999] show a concentration of flashes over Southeast Asia. The weaker chemical signatures of the Australia/Southeast Asian parcels compared to long-range parcels probably result from the relatively small amount of biomass burning over Southeast Asia [*Elvidge and Baugh*, 1996] compared to Africa and northern South America [*Fishman et al.*, 1996; European Space Agency, 1998].

Chemical data for the Australian/Southeast Asian category (Table 6) suggest some convective influence. Values of NO_x are comparable with those of the long-range category (Table 4); however, values of PAN and HNO_3 are smaller. Thus the enhanced $NO_x/\Sigma NO_i$ ratio mentioned above is due to small mixing ratios of PAN and HNO_3 and "fresh" NO and NO_2 from either a lightning or surface source. The organic acids, HCOOH and CH_3COOH, also are small, and together with small HNO_3 and moderate H_2O_2 indicate convective outflow. Figure 4c, showing vertical motion along the transport paths, indicates initially upward moving air whose altitude peaks near day 5, followed by slow subsidence to the point of measurement (the flight track). These ascent rates were not sufficient to exceed the 8°C/d potential temperature threshold. Therefore the trajectories passed the nonconvective criteria, although certain chemical tracers would argue otherwise.

6. Characteristics of Australian Air

The 17 trajectory clusters comprising the Australian category (Figure 3e) extend west of 155°E (over Australia) but do not pass over any other land mass within 10 days of arriving at the flight tracks. Figure 4d shows altitudes of Australian trajectories as a function of arrival time at the DC-8 location. These trajectories represent seven different flights. Their arrival altitudes (5.5 km, Table 2) and altitudes over the east coast of Australia (7.4 km) are considerably lower than those of the other categories. The Australian trajectories pass over the east coast of Australia ~4.8 days prior to reaching the DC-8 location, much later than passage times for the Southeast Asian (~1.6 days) and long-range categories (~1.9 days). Slower wind speeds at these lower altitudes explain the longer times, shorter trajectory paths (~12,350 km), and resulting lack of passage over other land areas. The median trajectory speed is 14 m s^{-1}.

The latitude at which trajectories pass Australia (20.4°S) is slightly south of that for the Southeast Asian trajectories (18.7°S), but farther north than the long-range trajectories (26.2°S). This latitude is near the boundary between the prevailing westerlies and tropical easterlies, explaining why some trajectories begin to turn anticyclonically toward Southeast Asia near the start of the 10-day period (Figure 3e).

Median mixing ratios for the Australian category (Table 7)

include O_3 (62 ppbv), CO (75 ppbv), HNO_3 (180 pptv), PAN (77 pptv), NO (14 pptv), and NO_x (27 pptv). Interquartile ranges for CO and C_2H_2 in the Australian category are similar to those of the long-range category (Table 4) (i.e., CO 66–84 ppbv Australian versus 60–84 ppbv long range, and C_2H_2 58–101 pptv Australian versus 54–107 pptv long range). This similarity suggests that the influence of biomass burning on the Australian category is approximately as strong as on the long-range category. The difference in lifetimes of CO and C_2H_2 due to altitude is only approximately 20% [*Schultz et al.*, 1999]. Therefore the similar C_2H_2/CO ratios between the long-range and Australian categories (1.1 pptv/ppbv) suggests that both groups of parcels receive emissions 5–7 days prior to reaching the flight track. In the case of the Australian parcels this timing is consistent with trajectory passage over the east coast of Australia (4.8 days, Table 2). On the other hand, the value of ΣNO_i is smaller in the Australian category, probably due to the smaller amount of biomass burning over Australia [*Hurst et al.*, 1996] than over southern Africa [*Fishman et al.*, 1996; *Olson et al.*, 1999]. Although enhanced scavenging of HNO_3 at the lower altitudes of the Australian category also could explain the smaller values of ΣNO_i, that scenario appears unlikely because mixing ratios of the soluble acidic gases HCOOH and CH_3COOH are somewhat greater than those of the long-range category. Nonetheless, as noted earlier, satellite imagery does show scattered deep convection over parts of Australia during PEM-T. Values of PAN and the ratio $NO_x/\Sigma NO_i$ are considerably smaller in the Australian category than in the long-range category due to the increased chemical loss of NO_x at the lower altitudes.

The difference in O_3 between the two categories (82 ppbv long range versus 62 ppbv Australian) is greater than expected solely from their differing altitudes. For example, *Schultz et al.* [1999] reported the net production rate of O_3 to be ~+1 ppbv/d at 10 km (long-range category) and ~0 at 6 km (Australian category). Integrated over the transport time from their source regions (5–7 days), altitude-related differences in O_3 would be only 5–7 ppbv if the initial concentrations of O_3 and its precursors were similar. The greater O_3 in the long-range category is consistent with the greater values of ΣNO_i, and this greater value also may reflect the stratospheric influence that was described earlier for that category.

The stronger chemical signatures of Australian parcels than the Australian/Southeast Asian parcels (Table 6) may be attributable to the lower altitudes of the Australian trajectories while passing over that continent. As noted earlier, satellite imagery shows scattered convection over Australia during PEM-T, but satellite-derived cloud-top temperatures (230–250 K) suggest typical heights of only 7–8 km. Thus by-products of biomass burning over Australia may have been convectively transported to altitudes of the Australian trajectories (~7.4 km), but not to the higher levels of the Australian/Southeast Asian parcels (11.6 km).

7. Characteristics of the Convective Category

The eighteen 10-day backward trajectory clusters comprising the convective category are shown in Figure 5a. These trajectories represent six different DC-8 flights. At least three of the five trajectories in each cluster experienced a diabatic change exceeding 10°C/d. They also passed through broad, persistent regions of satellite-observed convection usually associated with the SPCZ or ITCZ. Since 16 of the 18 trajectories remain over the ocean during their 10-day histories (Figure 5a), the category mostly represents marine convection. Satellite imagery and diabatic values reveal that the trajectories typically are influenced by that convection approximately 5 days prior to arriving at the DC-8 location. The arrival latitude (6.8°S, Table 2) is nearer the equator than any of the nonconvective categories. The median arrival altitude (11.2 km) is higher than that of any nonconvective category and significantly higher than their closest counterpart, the aged marine cases (6.5 km). Median altitudes at 5 and 10 days prior to arrival are 5.7 and 2.8 km, respectively. Most trajectories originate below 6 km, but then undergo rapid ascent while influenced by the convection (Figure 4e). This is opposite the overall weak subsidence encountered by the four categories of nonconvective clusters (Figures 4a–4d).

Table 7. Chemical Characteristics of Principle Species for 17 Australian Trajectory Clusters Representing Seven Different Flights

Species	LoQuart	Median	UpQuart	N
O_3	46	62	74	17
CO	66	75	84	17
C_2H_2	58	84	101	17
C_2H_2/CO	0.9	1.1	1.2	17
PAN	31	77	154	15
NO	10	14	19	15
NO_x	25	27	28	9
HNO_3	86	180	266	17
$NO_x/\Sigma NO_t$	0.08	0.08	0.09	5
HCOOH	64	147	281	17
CH_3COOH	70	91	159	17
H_2O_2	489	667	1503	17
CH_3OOH	201	255	576	14
H_2O_2/CH_3OOH	2.4	2.7	2.9	14
CH_3I	0.04	0.04	0.07	17
$CHBr_3$	0.31	0.36	0.43	17
^7Be	219	298	394	10
^{210}Pb	4.8	5.3	6.6	10
$RelHum_w$	7	10	18	16

Mixing ratios for chemicals are given in parts per trillion by volume (pptv), except for CO and O_3 which are in parts per billion by volume (ppbv), ^7Be and ^{210}Pb which are in fCi/scm, and relative humidity with respect to water (%). LOD values are in parentheses to indicate their contributions.

It is most appropriate to compare the chemical composition of this mostly marine convection category (Table 8) with that of the aged marine nonconvective category (Table 3). Mixing ratios of O_3 (33 ppbv) and CO (57 ppbv) are similar for the two categories. However, values of NO and NO_x for the convective category (29 and 25 pptv) are greater than those of aged marine air (6.8 and 10 pptv). The greater NO compared to NO_x is an artifact of the sampling; see the footnote to Table 7. Median NO = 20 pptv for the three samples of NO_x. The convective parcels may have received recent injections of NO from lightning associated with the convection [*Ehhalt et al.*, 1992; *Talbot et al.*, 1996b]. Specifically, *Fuelberg et al.* [1999] showed considerable lightning near and just east of Southeast Asia, but comparatively little lightning over the central Pacific near the ITCZ.

Mixing ratios of H_2O_2 and CH_3OOH in the convective category (244 and 148 pptv) are much smaller than in the aged marine category (701 and 388 pptv, respectively). Similarly, mixing ratios of HNO_3 and HCOOH are smaller (26 and 28 pptv compared to 52 and 37 pptv), while values of CH_3COOH

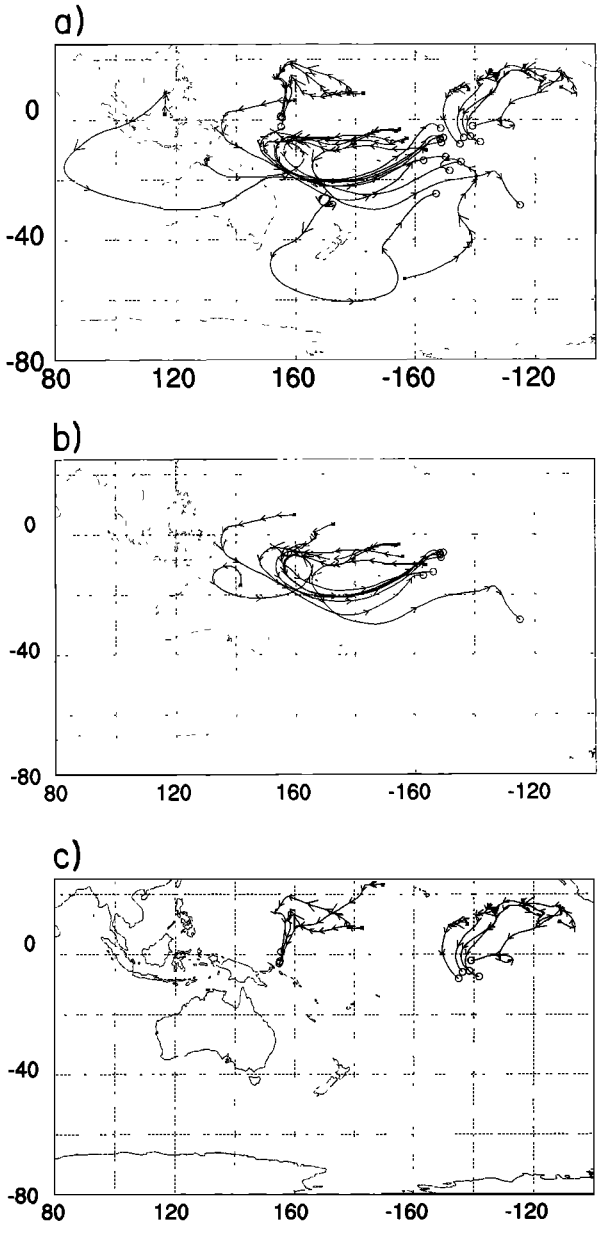

Figure 5. Trajectory paths of the convective categories: (a) all clusters, (b) SPCZ, and (c) ITCZ. For the sake of clarity, only one representative trajectory from each cluster is plotted.

are similar. Mixing ratios of ^{7}Be and ^{210}Pb for the convective category (103 and 1.5 fCi/scm, respectively) are smaller than those of the aged marine clusters (220 and 2.2 fCi/scm). These results strongly suggest soluble gas and particle removal by precipitation in the convective parcels.

It is informative to compare mixing ratios of CH_3OOH, H_2O_2, and CH_3I in the convective category with those for aged marine nonconvection. The median mixing ratio of CH_3I (0.08 pptv) is identical in the two sets of trajectories. However, this is reasonable since the convective trajectories typically are influenced by convection ~5 days prior to arrival, whereas the lifetime of CH_3I is approximately 4 days. The convective signal in CH_3OOH also should diminish given its shorter lifetime of 1–2 days and mixing with background air. Background mixing ratios of CH_3OOH at 11.2 km (median sample altitude of the convective category) are expected to be considerably smaller than those at 6.5 km (median sample altitude of the aged marine nonconvective category). *Cohan et al.* [1999] gave a background mixing ratio of 80 pptv for the 8–12 km altitude region. *Heikes et al.* [1996a], *O'Sullivan et al.* [1999], and *Lee et al.* [1998] showed a factor of 2–3 decrease in observed CH_3OOH mixing ratios between 6–8 and 10–12 km in subtropical and tropical latitudes. This altitude variation, together with precipitation scavenging, also may explain the lower values of H_2O_2 observed in the convective category compared to the aged marine nonconvective category. The ratio H_2O_2 to CH_3OOH appears to be more robust than the individual species for identifying convectively influenced air parcels. Background ratios at 10–12 km are typically greater than 3 [*Heikes et al.*, 1996a; *O'Sullivan et al.*, 1999; *Cohan et al.*, 1999; *Lee et al.*, 1998]. The median ratio of 1.3 for the convective category is much smaller than the background value at 10–12 km and is similar to that expected for convection with precipitation-influenced air parcels [*Heikes et al.*, 1996a; *Pickering et al.*, 1996].

Mixing ratios of CH_3OOH, H_2O_2, $CHBr_3$, and CH_3I from our trajectory-derived convection classification are considerably smaller than those presented by *Cohan et al.* [1999] using chemical criteria to identify "fresh" or "aged" convective outflow. Specifically, our values are intermediate between their outflow categories and background air category. This is expected since, as noted above, the trajectory clusters are influenced by convection ~5 days prior to arrival. The photochemical lifetimes of CH_3OOH, H_2O_2, $CHBr_3$, and CH_3I previously were noted to be 1–2, 3–5, >4, and 4 days, respectively. Thus a substantial portion of their chemical convective signal could be lost in 5 days.

We briefly consider two subsets of the convective category, trajectories passing through either the SPCZ or ITCZ, noting

Table 8. Chemical Characteristics of Principle Species for 18 Convective Trajectory Clusters Representing Six Different Flights

Species	LoQuart	Median	UpQuart	N
O_3	30	33	38	18
CO	55	57	61	15
C_2H_2	34	37	43	12
C_2H_2/CO	0.68	0.71	0.71	9
PAN	16	25	48	16
NO	11	29*	55	13
NO_x	22	25*	29	3
HNO_3	21	26	44	14
$NO_x/\Sigma NO_y$	...	...	...	0
HCOOH	20	28	33	14
CH_3COOH	20	35	39	13
H_2O_2	98	244	285	16
CH_3OOH	76	148	236	12
H_2O_2/CH_3OOH	1.0	1.3	1.9	12
CH_3I	0.03	0.08	0.11	12
$CHBr_3$	0.31	0.41	0.50	12
^{7}Be	(100)	103	302	12
^{210}Pb	1.2	1.5	2.3	12
$RelHum_w$	14	18	27	18

Mixing ratios for chemicals are given in parts per trillion by volume (pptv), except for CO and O_3 which are in parts per billion by volume (ppbv), ^{7}Be and ^{210}Pb which are in fCi/scm, and relative humidity with respect to water (%). LOD values are in parentheses to indicate their contributions.

*Only three samples included both a NO and NO_x measurement. The median NO_x of the three samples is 25 pptv, and the median NO is 20 pptv.

that the available data include only 7 or 8 samples representing two or three flights. The seven trajectory clusters comprising the SPCZ subcategory (Figure 5b) pass through the SPCZ and its associated convection. Satellite imagery and diabatic rates indicate that these trajectories typically are convectively influenced ~6 days prior to reaching the flight track. As observed with the overall convective category, these parcels experience considerable ascent while traveling toward the flight track (rising from 3.3 to 11.8 km during the 10-day period, not shown). Figure 5c shows trajectories for the eight clusters, which experience convection near the ITCZ (located near 10°N). These trajectories reach the flight track at a median latitude of 2.9°S and a median altitude of 11.3 km. Ascending motion in the convective region causes their median altitudes to increase from 2.4 to 11.3 km during the 10-day period (not shown).

Mixing ratios of acids and peroxides are quite small in the SPCZ category (Table 9), again indicating convective scavenging. In fact, mixing ratios of H_2O_2 and CH_3OOH (78 and 84 pptv, respectively) are smaller than those of the overall convective category (244 and 148 pptv, respectively). This is consistent with satellite imagery which shows that convective parcels within the SPCZ experience convection that is stronger and more widespread than convection in other locations (e.g., along the ITCZ). Mixing ratios of HNO_3, HCOOH, and CH_3COOH (23, 20, and 20 pptv, respectively) for the SPCZ parcels are smaller than those of the overall convective category (26, 28, and 35 pptv). These values also suggest more vigorous convective scavenging and/or greater convective coverage. In addition, the ratio H_2O_2/CH_3OOH (0.99) suggests that the convective influence is more recent than in the overall convective category (ratio equal to 1.3) [*Heikes*, 1992]. However, diabatic rates of individual SPCZ parcels and satellite imagery do not suggest a more recent convective influence within SPCZ parcels (~6 days) as compared to all convective trajectories (~5 days). On the other hand, the mixing ratio of NO (54 pptv) is much greater than within the overall convective category (29 pptv) and raises the issue about the relative importance of the effects of lightning associated within the SPCZ parcels. A larger database is needed to resolve some of these observations and differences.

Table 9. Chemical Characteristics of Principle Species for Seven SPCZ Trajectory Clusters Representing Three Different Flights

Species	LoQuart	Median	UpQuart	N
O_3	32	33	34	7
CO	50	51	53	4
C_2H_2	34	34	37	7
C_2H_2/CO	0.68	0.68	0.69	4
PAN	17	20	25	6
NO	34	54	66	6
NO_x	...	...	...	0
HNO_3	21	23	34	6
$NO_x/\Sigma NO_t$	...	...	...	0
HCOOH	16	20	25	6
CH_3COOH	20	20	31	6
H_2O_2	61	78	196	7
CH_3OOH	82	84	106	5
H_2O_2/CH_3OOH	0.96	0.99	1.2	5
CH_3I	0.03	0.04	0.07	7
$CHBr_3$	0.32	0.43	0.47	7
^7Be	(100)	(100)	(100)	6
^{210}Pb	1.2	1.2	1.7	6
$RelHum_w$	17	22	31	7

Mixing ratios for chemicals are given in parts per trillion by volume (pptv), except for CO and O_3 which are in parts per billion by volume (ppbv), ^7Be and ^{210}Pb which are in fCi/scm, and relative humidity with respect to water (%). LOD values are in parentheses to indicate their contributions.

Table 10. Chemical Characteristics of Principle Species for Eight ITCZ Trajectory Clusters Representing Two Different Flights

Species	LoQuart	Median	UpQuart	N
O_3	27	28	52	8
CO	56	57	60	8
C_2H_2	38	43	43	3
C_2H_2/CO	0.64	0.71	0.71	3
PAN	15	29	66	7
NO	18	30	46	4
NO_x	25	25	25	1
HNO_3	26	28	127	7
$NO_x/\Sigma NO_t$	...	...	...	0
HCOOH	28	30	44	7
CH_3COOH	34	38	44	7
H_2O_2	234	265	302	8
CH_3OOH	107	198	242	7
H_2O_2/CH_3OOH	1.2	1.7	3.7	7
CH_3I	0.14	0.15	0.15	3
$CHBr_3$	0.34	0.38	0.46	3
^7Be	234	504	583	5
^{210}Pb	1.5	2.4	2.9	5
$RelHum_w$	14	17	22	8

Mixing ratios for chemicals are given in parts per trillion by volume (pptv), except for CO and O_3 which are in parts per billion by volume (ppbv), ^7Be and ^{210}Pb which are in fCi/scm, and relative humidity with respect to water (%). LOD values are in parentheses to indicate their contributions.

Many chemical characteristics of the ITCZ category (Table 10) are similar to those of the SPCZ category (Table 9). However, there are several notable differences. The median value of CH_3I (0.15 pptv) is greater in the ITCZ group than in the SPCZ grouping. This suggests a more recent marine convective signature (within 2–5 days) [*Cohan et al.*, 1999]. On the other hand, the greater ratio H_2O_2/CH_3OOH (1.7 versus 1.3) suggests a longer time since convection. The median mixing ratio of $CHBr_3$ (0.38 pptv) is approximately the same as those of the nonconvective categories, not supporting a marine convective signature [*Cohan et al.*, 1999]. Although this might indicate a biomass burning influence, that is not supported by the small median values of O_3 and CO (28 and 57 ppbv, respectively). Median mixing ratios of HNO_3 (28 pptv), HCOOH (30 pptv), CH_3COOH (38 pptv), and ^7Be (504 fCi/scm) are considerably greater than those of the SPCZ category. In general, these values suggest that parcels encountering the ITCZ experience a less pronounced convective signature than trajectories encountering the SPCZ. This is consistent with less widespread convection over the ITCZ than SPCZ. However, once again, a larger database is necessary to confirm these observations.

8. Conclusions

Chemical data gathered by NASA's DC-8 aircraft as well as 10-day backward trajectories have been used to examine atmospheric chemistry over the tropical Pacific Basin during NASA's PEM-T field project (August–October 1996). Trajectory arrival locations were along flight tracks of the DC-8 where coincident time-averaged chemical data were available.

A series of quality control tests determined the most reliable trajectories. Temporal changes in potential temperature were used to determine whether trajectories experienced a significant convective influence during the 10-day period.

Trajectories designated nonconvective were required to have a consistent geographical origin and experience a 24 hour change in potential temperature less than 8°C/d. Conversely, convective trajectories were required to experience >10°C change in 24 hours, to pass through extensive satellite-indicated convection, and to have a consistent geographical origin. The nonconvective group was subdivided into four geographical categories representing source region and transport history as follows: (1) aged marine, (2) long-range, (3) Australia/Southeast Asia, and (4) Australia. The convective group was divided into two geographical categories representing the location of the widespread convection, that is, along either the SPCZ or ITCZ. Thus the convective groups mostly represent parcels experiencing marine convection. Chemical characteristics of the geographically based categories were compared, and trajectory data and satellite imagery were used to interpret the chemical results. One should note that our methodology is the reverse of using trajectories to determine the origin of air having a particular chemical signature.

The major finding is that chemical characteristics of the various categories are consistent with information from the trajectories, that is, their source regions, 10-day transport paths, and atmospheric processing (e.g., major convection and lightning). The aged marine category had relatively small mixing ratios of O_3, CO, HNO_3, and PAN (medians of 34 ppbv, 56 ppbv, 52 pptv, and 16 pptv, respectively), indicating the absence of a significant continental influence. The C_2H_2/CO ratio was approximately 0.6 (pptv/ppbv). Although these trajectories arrived at a wide variety of aircraft sampling altitudes, they all remained far from land sources, explaining their aged marine character.

Compared to aged marine air, the long-range trajectory category exhibited a stronger pollution signature. This category included parcels that passed over Australia, southern Africa, and in some cases even South America. Median values of O_3, CO, HNO_3, and PAN were 82 ppbv, 70 ppbv, 145 pptv, and 105 pptv, respectively. These long-range trajectories were at relatively high altitudes (10–11 km) as they traveled the long distances to the PEM-T DC-8 measurement locations. The chemical signature of the long-range category is consistent with biomass burning. The signature is most consistent with injection of biomass emissions over Africa and South America 5–7 days prior to measurement, as opposed to injection over Australia ~2 days prior to measurement. A subset of the long-range trajectories, that is, those that extended to northern South America within 10 days, generally exhibited more impact from biomass burning than parcels in the overall category (most of which did not reach South America within 10 days). Previous studies of the PEM-T data have given convincing evidence that the study area was impacted by biomass burning emissions, and not urban emissions [e.g., *Schultz et al.*, 1999] (and other papers in the first PEM-T special section of the *Journal of Geophysical Research*, 1998). Our analyses support that conclusion. Large values of ^7Be (median equal to 1000 fCi/scm) probably are due to either less efficient removal of aerosols from upper tropospheric air or to small stratospheric contributions.

Air parcels in the Australia/Southeast Asian category were located over Southeast Asia 7–10 days prior to measurement and over Australia ~1.6 days prior to measurement. The trajectories traveled at relatively high altitudes (9–15 km). These parcels exhibited a weak pollution signature, as suggested by O_3, CO, HNO_3, and PAN mixing ratios of 46 ppbv, 67 ppbv, 51 pptv, and 38 pptv, respectively. These values are slightly greater than those of aged marine parcels, but significantly smaller than those of the long-range and Australian groups. Their reduced chemical signature is attributed to limited burning over Southeast Asia and their relatively high transport altitude over biomass burning regions of Australia. There was evidence of convection and lightning in some of the chemical species.

Parcels in the Australian category passed over the eastern coast of that continent ~5 days prior to measurement, having traversed no other land mass during the 10-day period. Median mixing ratios of O_3, CO, HNO_3, and PAN (62 ppbv, 75 ppbv, 180 pptv, and 77 pptv, respectively) were greater than those of aged marine parcels. Values of CO and C_2H_2 (84 pptv) suggest a biomass burning influence that is approximately as strong as in the long-range category. However, photochemical product species such as O_3 and PAN are smaller than in the long-range transport category. These trajectories traveled at considerably lower altitudes (~7 km) and therefore at slower speeds than the long-range trajectories. We believe that their chemical signature is impacted mainly by biomass burning in Australia whose emissions would reach the relatively low transport altitudes over Australia. That is, since the convection over Australia had tops between 7 and 8 km, the burning by-products could be lofted to heights of the trajectories. This scenario seems unlikely for the long-range and Southeast Asian categories since those trajectories pass over Australia at much higher altitudes (10–12 km). Although the Australian parcels may have traversed Africa prior to 10 days, that is before our analysis period. Thus it is not known whether African or South American emissions significantly affected the observed chemistry of the Australian category. The C_2H_2/CO ratios indicated that parcels were influenced by combustion approximately 5–7 days prior to their flight track arrivals, agreeing with trajectory passage times over Australia.

Chemical signatures of trajectories experiencing a major convective influence were consistent with that categorization. Most of the convection occurred along the ITCZ or SPCZ, that is, marine convection. Satellite imagery and diabatic rates revealed that the air parcels were influenced by convection approximately 5 days prior to arriving at the DC-8 sampling locations. Most of the trajectories originated below 6 km altitude, experienced rapid ascent while convectively influenced, and arrived at the DC-8 flight track at approximately 10–11 km altitude. Mixing ratios of peroxides (H_2O_2 and CH_3OOH) and acids (HNO_3, HCOOH, and CH_3COOH) for the convective parcels were depleted (typically factors of 2 smaller than aged marine air). Mixing ratios of ^7Be and ^{210}Pb also were smaller for the convective air, and when combined with results of the peroxides and acids, suggest soluble and particle removal by precipitation in the convective region. The 5-day time of convection (prior to DC-8 sampling) negates meaningful results from shorter-lived marine tracers (e.g., CH_3I and $CHBr_3$). When the convective category was subdivided according to the location where convection was encountered (near the ITCZ or SPCZ), the chemical, satellite, and meteorological data all suggested more active convection and removal processes in the region of the SPCZ compared to the ITCZ. However, a larger database is required to discern regional differences.

Current results indicate that the merging of trajectory and chemical information is a valuable tool for understanding chemical measurements. The findings suggest that if one uses careful screening procedures, trajectories can be a reliable indicator of air parcel origins and atmospheric mixing during transport.

Acknowledgments. This research was funded by NASA's Tropospheric Chemistry Program. David Westberg and Robert Chatfield provided archived satellite data.

References

Andreae, M. O., et al., Methyl halide emissions from savanna fires in southern Africa, *J. Geophys. Res.*, *101*, 23,603–23,613, 1996.

Bengtsson, L., Medium-range forecasting—The experience of ECMWF, *Bull. Am. Meteorol. Soc.*, *66*, 1133–1146, 1985.

Bhandari, N., D. Lal, and Rama, Stratospheric circulation studies based on natural and artificial radioactive tracer elements, *Tellus*, *18*, 391–405, 1966.

Blake, N. J., D. R. Blake, B. C. Sive, T.-Y. Chen, F. S. Rowland, J. E. Collins Jr., G. W. Sachse, and B. E. Anderson, Biomass burning emissions and vertical distribution of atmospheric methyl halides and other reduced carbon gases in the South Atlantic region, *J. Geophys. Res.*, *101*, 24,151–24,164, 1996.

Chatfield, R. B., and A. C. Delany, Convection links biomass burning to increased tropical ozone: However, models will tend to overpredict O_3, *J. Geophys. Res.*, *95*, 18,473–18,488, 1990.

Cohan, D. S., M. G. Schultz, D. J. Jacob, B. G. Heikes, and D. R. Blake, Convective injection and photochemical decay of peroxides in the tropical upper troposphere: Methyl iodide as a tracer of marine convection, *J. Geophys. Res.*, *104*, 5717–5724, 1999.

Dibb, J. E., R. W. Talbot, K. I. Klemm, G. L. Gregory, H. B. Singh, J. D. Bradshaw, and S. T. Sandholm, Asian influence over the western North Pacific during the fall season: Inferences from lead 210, soluble ionic species, and ozone, *J. Geophys. Res.*, *101*, 1779–1792, 1996.

Dibb, J. E., R. W. Talbot, L. D. Meeker, E. Scheuer, N. J. Blake, D. R. Blake, G. L. Gregory, and G. W. Sachse, Constraints on the age and dilution of PEM-Tropics biomass burning plumes from the natural radionucleide tracer ^{210}Pb, *J. Geophys. Res.*, this issue.

Doty, K. G., and D. J. Perkey, Sensitivity of trajectory calculations to the temporal frequency of wind data, *Mon. Weather Rev.*, *121*, 387–401, 1993.

Draxler, R. R., The accuracy of trajectories during ANATEX calculated using dynamic model analyses versus rawinsonde observations, *J. Appl. Meteorol.*, *30*, 1446–1467, 1991.

Ehhalt, D. W., F. Roher, and A. Wahner, Sources and distributions of NO_x in the upper troposphere at northern midlatitudes, *J. Geophys. Res.*, *97*, 9781–9793, 1992.

Elbern, H., J. Kowol, R. Sladkovic, and A. Ebel, Deep stratospheric intrusions: A statistical assessment with model guided analyses, *Atmos. Environ.*, *31*, 3207–3226, 1997.

Elvidge, C. D., and K. E. Baugh, Survey of fires in Southeast Asia and India during 1987, in *Biomass Burning and Global Change*, edited by J. S. Levine, pp. 663–670, MIT Press, Cambridge, Mass., 1996.

Fishman, J., K. Fakhruzzaman, B. Cros, and D. Nganga, Identification of widespread pollution in the southern hemisphere deduced from satellite analyses, *Science*, *252*, 1693–1696, 1991.

Fishman, J., J. M. Hoell Jr., R. D. Bendura, R. J. McNeal, and V. W. J. H. Kirchhoff, NASA GTE TRACE A Experiment (September–October 1992): Overview, *J. Geophys. Res.*, *101*, 23,865–23,879, 1996.

Fuelberg, H. E., J. D. Van Ausdall, E. V. Browell, and S. P. Longmore, Meteorological conditions associated with vertical distributions of aerosols off the west coast of Africa, *J. Geophys. Res.*, *101*, 24,105–24,115, 1996a.

Fuelberg, H. E., R. O. Loring Jr., M. V. Watson, M. C. Sinha, K. E. Pickering, A. M. Thompson, G. W. Sachse, D. R. Blake, and M. R. Schoeberl, TRACE A trajectory intercomparison, 2, Isentropic and kinematic methods, *J. Geophys. Res.*, *101*, 23,927–23,939, 1996b.

Fuelberg, H. E., R. E. Newell, S. P. Longmore, Y. Zhu, D. J. Westberg, E. V. Browell, D. R. Blake, G. L. Gregory, and G. W. Sachse, A meteorological overview of the Pacific Exploratory Mission (PEM) Tropics period, *J. Geophys. Res.*, *104*, 5585–5622, 1999.

Garstang, M., P. D. Tyson, R. Swap, M. Edward, P. Kallberg, and A. J. Lindesay, Horizontal and vertical transport of air over southern Africa, *J. Geophys. Res.*, *101*, 23,721–23,736, 1996.

Greenberg, J. P., and P. R. Zimmerman, Nonmethane hydrocarbons in remote tropical, continental, and maritime atmospheres, *J. Geophys. Res.*, *89*, 4764–4778, 1984.

Greenberg, J. P., P. R. Zimmerman, and P. Haagenson, Tropospheric hydrocarbons and CO profiles over the U.S. West Coast and Alaska, *J. Geophys. Res.*, *95*, 14,015–14,026, 1990.

Gregory, G. L., H. E. Fuelberg, S. P. Longmore, B. E. Anderson, J. E. Collins, and D. R. Blake, Chemical characteristics of tropospheric air over the tropical South Atlantic Ocean: Relationship to trajectory history, *J. Geophys. Res.*, *101*, 23,957–23,972, 1996.

Gregory, G. L., et al., Chemical characteristics of Pacific tropospheric air in the region of the Intertropical Convergence Zone and South Pacific Convergence Zone, *J. Geophys. Res.*, *104*, 5677–5696, 1999.

Hao, W. M., and M.-H. Liu, Spatial and temporal distribution of tropical biomass burning, *Global Biogeochem. Cycles*, *8*, 495–503, 1994.

Harriss, R. C., G. W. Sachse, G. F. Hill, L. Wade, K. E. Bartlett, J. E. Collins, L. F. Steels, and P. C. Novelli, Carbon monoxide and methane in the North American Arctic and subarctic troposphere: July–August 1988, *J. Geophys. Res.*, *97*, 16,589–16,599, 1992.

Heikes, B. G., Formaldehyde and hydroperoxides at Mauna Loa Observatory, *J. Geophys. Res.*, *97*, 18,001–18,013, 1992.

Heikes, B. G., et al., Hydrogen peroxide and methylhydroperoxide distributions related to ozone and odd hydrogen over the North Pacific in the fall of 1991, *J. Geophys. Res.*, *101*, 1891–1905, 1996a.

Heikes, B. G., et al., Ozone hydroperoxides, oxides of nitrogen, and hydrocarbon budgets in the marine boundary layer over the South Atlantic, *J. Geophys. Res.*, *101*, 24,221–24,234, 1996b.

Hoell, J. M., D. D. Davis, D. J. Jacob, M. O. Rodgers, R. E. Newell, H. E. Fuelberg, R. J. McNeal, J. L. Raper, and R. J. Bendura, Pacific Exploratory Mission in the tropical Pacific: PEM-Tropics A, August–September 1996, *J. Geophys. Res.*, *104*, 5567–5583, 1999.

Hollingsworth, A., D. B. Shaw, P. Lonnberg, L. Illari, K. Arpe, and A. J. Simmons, Monitoring of observations and analysis quality by a data assimilation system, *Mon. Weather Rev.*, *114*, 861–879, 1986.

Hurst, D. F., D. W. T. Griffith, and G. D. Cook, Trace-gas emissions from biomass burning in Australia, in *Biomass Burning and Global Change*, edited by J. S. Levine, pp. 787–792, MIT Press, Cambridge, Mass., 1996.

Jaeglé, L., et al., Observed OH and H_2O_2 in the upper troposphere suggests a major source from convective injection of peroxides, *Geophys. Res. Lett.*, *24*, 3181–3184, 1997.

Justice, C. O., J. D. Kendall, P. R. Dowty, and R. J. Scholes, Satellite remote sensing of fires during the SAFARI campaign using NOAA advanced very high resolution radiometer data, *J. Geophys. Res.*, *101*, 23,851–23,864, 1996.

Kawa, S. R., and R. Pearson Jr., Ozone budgets from the dynamics and chemistry of marine stratocumulus experiment, *J. Geophys. Res.*, *94*, 9809–9817, 1989.

Krishnamurti, T. N., H. E. Fuelberg, M. C. Sinha, D. Oosterhof, E. L. Bensman, and V. B. Kumar, The meteorological environment of the tropospheric ozone maximum over the tropical South Atlantic Ocean, *J. Geophys. Res.*, *98*, 10,621–10,641, 1993.

Kritz, M. A., S. W. Rosner, E. F. Danielsen, and H. B. Selkirk, Air mass origins and troposphere-to-stratosphere exchange associated with midlatitude cyclogenesis and tropopause folding inferred from Be-7 measurements, *J. Geophys. Res.*, *96*, 17,405–17,414, 1991.

Lee, M., B. G. Heikes, and D. J. Jacob, Enhancements of hydroperoxides and formaldehyde in biomass burning impacted air and their effect on atmospheric oxidant cycles, *J. Geophys. Res.*, *103*, 13,201–13,212, 1998.

Liu, S. C., M. Trainer, F. C. Fehsenfeld, D. D. Parrish, E. J. Williams, D. W. Fahey, G. Hubler, and P. C. Murphy, Ozone production in the rural troposphere and the implications for regional and global ozone distributions, *J. Geophys. Res.*, *92*, 4191–4207, 1987.

Liu, S. C., et al., A model study of tropospheric trace species distributions during PEM-West A, *J. Geophys. Res.*, *101*, 2073–2085, 1996.

McKeen, S. A., and S. C. Liu, Hydrocarbon ratios and photochemical history of air masses, *Geophys. Res. Lett.*, *20*, 2363–2366, 1993.

McKeen, S. A., S. C. Liu, E.-Y. Hsie, X. Lin, J. B. Bradshaw, S. Smyth, G. L. Gregory, and D. R. Blake, Hydrocarbon ratios during PEM-

West A: A model perspective, *J. Geophys. Res.*, *101*, 2087–2109, 1996.

Merrill, J. T., R. Bleck, and L. Avila, Modeling atmospheric transport to the Marshall Islands, *J. Geophys. Res.*, *90*, 12,927–12,936, 1985.

Olson, J. R., B. A. Baum, D. R. Cahoon, and J. H. Crawford, Frequency and distribution of forest, savanna, and crop fires over tropical regions during PEM-Tropics A, *J. Geophys. Res.*, *104*, 5865–5876, 1999.

O'Sullivan, D. W., B. G. Heikes, M. Lee, W. Chang, G. L. Gregory, D. R. Blake, and G. W. Sachse, Distribution of hydrogen peroxide and methylhydroperoxide over the Pacific and South Atlantic Oceans, *J. Geophys. Res.*, *104*, 5635–5646, 1999.

Pickering, K. E., A. M. Thompson, R. R. Dickerson, W. T. Luke, D. P. McNamara, J. P. Greenberg, and P. R. Zimmerman, Model calculations of tropospheric ozone production potential following observed convective events, *J. Geophys. Res.*, *95*, 14,049–14,062, 1990.

Pickering, K. E., A. M. Thompson, J. R. Scala, W.-K. Tao, J. Simpson, and M. Garstang, Photochemical ozone production in tropical squall line convection during NASA Global Tropospheric Experiment/Amazon Boundary Layer Experiment 2A, *J. Geophys. Res.*, *96*, 3099–3144, 1991.

Pickering, K. E., A. M. Thompson, J. R. Scala, W.-K. Tao, and J. Simpson, Ozone prediction potential following convective redistributions of biomass burning emissions, *J. Atmos. Chem.*, *14*, 297–313, 1992.

Pickering, K. E., et al., Convective transport of biomass burning emissions over Brazil during TRACE A, *J. Geophys. Res.*, *101*, 23,993–24,012, 1996.

Ridley, B. A., et al., Ratios of peroxyacetyl nitrate to active nitrogen observed during aircraft flights over the eastern Pacific Ocean and continental United States, *J. Geophys. Res.*, *95*, 10,179–10,192, 1990.

Rood, R. B., A. R. Douglass, M. C. Cerniglia, and W. B. Read, Synoptic-scale mass exchange from the troposphere to the stratosphere, *J. Geophys. Res.*, *102*, 23,467–23,485, 1997.

Scala, J. R., et al., Cloud draft structure and trace gas transport, *J. Geophys. Res.*, *95*, 17,015–17,030, 1990.

Schultz, M. G., et al., On the origin of tropospheric ozone and NO_x over the tropical South Pacific, *J. Geophys. Res.*, *104*, 5829–5843, 1999.

Singh, H. B., and P. B. Zimmerman, Atmospheric distribution and sources of nonmethane hydrocarbons, *Adv. Environ. Sci. Technol.*, *24*, 177–235, 1992.

Singh, H. B., et al., Peroxyacetyl nitrate measurements during CITE 2: Atmospheric distribution and precursor relationships, *J. Geophys. Res.*, *95*, 10,163–10,178, 1990.

Smyth, S., et al., Comparison of free tropospheric western Pacific air mass classification schemes for the PEM-West A experiment, *J. Geophys. Res.*, *101*, 1743–1762, 1996.

Stohl, A., G. Wotawa, P. Seibert, and H. Kromp-Kolb, Interpolation errors in wind fields as a function of spatial and temporal resolution and their impact on different types of kinematic trajectories, *J. Appl. Meteorol.*, *34*, 2149–2165, 1995.

Swap, R., M. Garstang, S. A. Macko, P. D. Tyson, W. Maenhaut, P. Artaxo, P. Kallberg, and R. Talbot, The long-range transport of southern African aerosols to the tropical South Atlantic, *J. Geophys. Res.*, *101*, 23,777–23,791, 1996.

Talbot, R. W., M. O. Andreae, H. Berresheim, D. J. Jacob, and K. M. Beecher, Sources and sinks of formic, acetic, and pyruvic acids over central Amazonia, 2, Wet season, *J. Geophys. Res.*, *95*, 16,779–16,812, 1990.

Talbot, R. W., et al., Summertime distribution and relations of reactive odd nitrogen species and NO_y in the troposphere over Canada, *J. Geophys. Res.*, *99*, 1863–1885, 1994.

Talbot, R. W., et al., Chemical characteristics of continental outflow from Asia to the troposphere over the western Pacific Ocean during September–October 1991: Results from PEM-West A, *J. Geophys. Res.*, *101*, 1713–1725, 1996a.

Talbot, R. W., et al., Chemical characteristics of continental outflow over the tropical South Atlantic Ocean from Brazil and Africa, *J. Geophys. Res.*, *101*, 24,187–24,202, 1996b.

Talbot, R. W., et al., Chemical characteristics of continental outflow from Asia to the troposphere over the western Pacific Ocean during February–March 1994: Results from PEM-West B, *J. Geophys. Res.*, *102*, 28,255–28,274, 1997.

Thompson, A. M., K. E. Pickering, D. P. McNamara, M. R. Schoeberl, R. D. Hudson, J. H. Kim, E. V. Browell, V. W. J. H. Kirchoff, and D. Nganga, Where did tropospheric ozone over southern Africa and tropical Atlantic come from in October 1992? Insights from TOMS, GTE TRACE A, and SAFARI 1992, *J. Geophys. Res.*, *101*, 24,251–24,278, 1996.

Turekian, K. K., W. C. Graustein, and J. K. Cochran, Lead-210 in the SEAREX program: An aerosol tracer across the Pacific, in *Chemical Oceanography*, vol. 10, edited by J. P. Riley, R. Chester, and R. A. Duce, pp. 51–80, Academic, San Diego, Calif., 1989.

Tyson, P. D., M. Garstang, R. Swap, P. Kallberg, and M. Edwards, An air transport climatology for subtropical southern Africa, *Int. J. Climatol.*, *16*, 2165–2191, 1996.

Vay, S. A., B. E. Anderson, T. J. Conway, G. W. Sachse, J. E. Collins Jr., D. R. Blake, and D. J. Westberg, Airborne observations of the tropospheric CO_2 distribution and its controlling factors over the South Pacific Basin, *J. Geophys. Res.*, *104*, 5663–5676, 1999.

Vincent, D. G., The South Pacific convergence zone: A review, *Mon. Weather Rev.*, *122*, 1949–1970, 1994.

D. R. Blake, Department of Chemistry, University of California, Irvine, CA 92717.

A. S. Board and H. E. Fuelberg (corresponding author), Department of Meteorology, Florida State University, Tallahassee, FL 32306-4520. (fuelberg@met.fsu.edu)

J. E. Dibb and R. W. Talbot, Institute for the Study of Earth, Oceans, and Space, University of New Hampshire, Durham, NH 03824.

G. L. Gregory, NASA Langley Research Center, Hampton, VA 23681.

B. G. Heikes, Graduate School of Oceanography, University of Rhode Island, Narragansett, RI 02882.

S. T. Sandholm, Department of Earth and Atmospheric Sciences, Georgia Institute of Technology, Atlanta, GA 30332.

M. G. Schultz, Department of Earth and Planetary Sciences, Harvard University, Cambridge, MA 02138.

(Received August 3, 1998; revised December 1, 1998;
accepted January 11, 1999.)